

Casimir Effect and Gravitational Balance: a Search for Stable Configurations

Leonardo Bellinato Giacomelli^{1,2}, Benjamin Koch ^{*1,4}, Iva Lovrekovic¹,
and Angel Rincon ^{†3}

¹Institut für Theoretische Physik, TU Wien, Wiedner Hauptstrasse 8-10,
1040 Vienna, Austria

²Universität Innsbruck, Fakultät für Mathematik, Informatik und Physik,
Institut für Experimentalphysik, 6020 Innsbruck, Austria

⁴Instituto de Física, Pontificia Católica Universidad de Chile, Av. Vicuña
Mackenna 4860, Santiago, Chile

³Departamento de Física Aplicada, Universidad de Alicante, Campus de
San Vicente del Raspeig, E-03690 Alicante, Spain.

July 2023

Abstract

In this study, we examine the role of the repulsive Casimir force in counteracting the gravitational contraction of a thin spherically symmetric shell. Our main focus is to explore the possibility of achieving a stable balanced configuration within the theoretically reliable weak field limit. To this end, we consider different types of Casimir forces, including those generated by massless scalar fields, massive scalar fields, electromagnetic fields, and temperature-dependent fields.

*E-mail: benjamin.koch@tuwien.ac.at

†E-mail: angel.rincon@ua.es

Contents

1	Introduction	3
1.1	Gravitational balance	3
1.2	Casimir effect	4
1.3	Thin shells as toy model for gravitational collapse	5
1.4	The research question	6
1.5	Structure of the paper	6
2	Results	7
2.1	The setup	7
2.2	Massless scalar field	9
2.3	Massive scalar field	13
2.4	Temperature dependence	16
2.4.1	High temperature for scalar field	17
2.4.2	Low temperature for scalar field	17
2.4.3	Electromagnetic Casimir at low temperature and large $R \gg r_S$. . .	19
3	Conclusion	21
4	Acknowledgements	22
	Bibliography	25

1 Introduction

1.1 Gravitational balance

Gravitational balance is a fascinating area of research within astrophysics and general relativity that explores the processes by which massive objects, such as stars, balance out with their gravitational force or collapse under it [1–7]. Research in this area continues to push the boundaries of our understanding of the universe, offering tantalizing prospects for breakthroughs in both the theoretical and observational realms. It pushes our understanding of the laws of nature to its boundaries.

Among the possible forces that might stabilize a gravitational system, one has considered electromagnetic forces, strong forces, the Pauli exclusion principle, and quantum vacuum energy. The former forces are directly associated with the coupling strength of the standard model of particle physics. The latter forces are of totally different nature, because their existence is directly linked to genuine quantum effects.

Among these candidate forces, the quantum vacuum energy is certainly the least explored and least understood. One reason for our limited knowledge of vacuum energy is certainly the difficulty in measuring it [8]. Another reason is the fact that the role of quantum vacuum energy is largely unclear when it is coupled to gravity. This lies at the core of the infamous cosmological constant problem. Which is the large discrepancy between the theoretical predictions of vacuum energy density from quantum field theory and the observed value of this density from astronomical observations at cosmological scales, which differ by approximately 120 orders of magnitude [9]. Understanding the interplay between vacuum energy density and gravity might also play a non-trivial role in the evolution process of compact gravitational objects [10, 11]. This is the region of high curvature that we do not explore here.

It is thus an interesting research objective to learn more about vacuum energy in general (see subsection 1.2) and in particular in the context of a gravitational collapse for the thin shells similar as in Israel (see 1.3 and the following). Due to the specific nature of the theory, we expect our observations to appear at extreme scales.

1.2 Casimir effect

Studies of the Casimir effect span multiple disciplines. It is important in quantum field theory, atomic and molecular physics, condensed matter physics, gravity and cosmology, mathematical physics, and others [12]. For instance, in Quantum Field Theory, bag models of hadrons, the Casimir modes of quarks, and gluons significantly contribute to the total nucleon energy. In Kaluza-Klein theory, the Casimir effect provides an effective mechanism for the spontaneous compactification of extra dimensions. In Condensed Matter Physics, the Casimir effect can be either attractive or repulsive between closely aligned material boundaries, strongly depending on the geometry of the boundaries, temperature, and the mechanical and electrical properties of the boundary surface [13].

In the bag model of Quantum Chromodynamics (QCD), the boundary conditions on the spinor and gluon fields are related through equations of motion. Essentially, there is a Lagrangian model for the bag, along with a phenomenological Lagrangian description for the quantum behavior of the fields within the bag. Although the MIT bag model, since its discovery long ago, has been largely replaced by newer methods in QCD to study hadrons, it was a successful phenomenological description in its time [14, 15]. The accuracy of this phenomenological effective description led to numerous discoveries [16, 17].

Boyer demonstrated the importance of geometry in calculating the Casimir force [18]. He investigated the quantum electromagnetic zero-point energy (known as the Casimir energy) of a conducting spherical shell. By analogy with the parallel plate configuration, he expected the negative contribution from zero-point energy to induce a collapse of the sphere, balanced by the electrostatic energy of the configuration. To his surprise, the Casimir energy contribution was positive. He considered quantum electromagnetic modes within the sphere. Further studies yielded interesting results on the dependence on geometry [12]. Specifically, the energy contribution for a rectangular cavity can vary between positive and negative values, depending on the dimensions of the cavity. In one case, it may be positive, while in another it may be negative.

There have been numerous studies on the conducting sphere initiated by Boyer [18] and followed by analyses using Green's function methods [19, 20]. These include the calculation of the vacuum energy for (i) spinors in the bag model [21, 22], (ii) massive scalar enclosed in the system [23], (iii) and for fermions [24]. For the massless scalar field

inside a sphere, the Casimir energy is given by

$$E_{Cas} = \frac{\hbar c}{R} \left(0.0044 + \frac{1}{630\pi} \left[\frac{1}{s} + \left(\frac{\mu c R}{\hbar} \right) \right] \right), \quad (1.1)$$

where sphere is of a radius R in $D=3$ dimensions with Dirichlet boundary conditions [13]. Also experimental studies of this effect are intensified recently [25].

In the gravitational case, the analysis of quantum modes within an analogous conducting sphere is more complex and has not been extensively considered. However, studies have been conducted on gravitons in the Casimir box, showing a linear dependence compared to the analysis for scalars. In the scenario with two infinite parallel planes separated by distance d , linearized gravity, similar to electromagnetism, can be represented as two free massless scalar fields?one with Neumann boundary conditions and one with Dirichlet boundary conditions. The calculated partition function can then be obtained also by studying a single massless scalar field on an interval of length $2d$ with periodic boundary conditions [26].

1.3 Thin shells as toy model for gravitational collapse

In this paper, on phenomenological grounds, we consider a scenario in which a thin spherical shell with non-vanishing mass counteracts the repulsive Casimir force due to its gravity. The Casimir energy arises from the fluctuations of the dynamical field both inside and outside the shell.

If we adopt the line of thinking used in the MIT bag model to a scenario involving gravity, we can attempt to model the interplay between zero-point energy and gravitational effects. To utilize the result for the Casimir energy of dynamical field inside a perfectly conducting sphere, we can imagine a model similar to a bag, but with quantum fluctuations occurring on both sides of the boundary. The sphere is massive and is described in flat space, experiencing gravitational effects due to its mass. In realistic physical scenarios, this description would be too simplistic. It would be necessary to carefully determine the energy of particles fluctuating within the system and the scale at which these fluctuations would be sufficient to counterbalance the mass.

A very instructive toy model in this direction was introduced by Brevik [27], where he included the contribution of Casimir energy to the gravitational system of a shell by hand. In his model, the shell contracts to a minimum radius, at which point it encounters

a barrier at the speed of light. Without the Casimir force, this setup would lead to the collapse of the shell.

1.4 The research question

As a toy model, we use a thin spherical shell that experiences both gravitational and vacuum effects simultaneously. A description of this system was already implemented by Brevik, as mentioned in the previous section [27]. In his work, the focus is on a regime of strong curvature and large velocities. However, in this regime, the Newtonian concept of simply summing forces to obtain a total force is likely not valid or is at least obscured by significant theoretical uncertainties.

Therefore, in our work, we will focus on a regime of low curvature and small velocities, where the Newtonian approach of adding the Casimir force to the gravitational equations of motion is certainly valid. Consequently, we concentrate on the following research question:

“Under which circumstances can Casimir forces counteract gravitational attraction and lead to stable configurations, even in the non-relativistic, low-curvature limit?”

In this regime of non-relativistic dynamics, we consider three distinct scenarios:

- α) The shell collapses, with gravitational forces overwhelming the Casimir force.
- β) The shell expands from its initial radius due to a stronger Casimir force.
- γ) The shell oscillates around a stable radius.

Our primary focus is to explore whether the dynamics of the Casimir shell is always destructive (either α or β), or if there exists a region in the parameter space and initial conditions where the shell is stable (γ). We will classify different regimes and types of Casimir forces according to the scenarios (α, β, γ) they produce for the spherical massive shell.

1.5 Structure of the paper

In the following section we will define the setup of a thin self-gravitating shell 2.1. Then, we will explore this system for different types of Casimir forces and categorize it into the

scenarios α , β , γ . In particular, we will consider a massless scalar field, a massive scalar field, and temperature dependence for massless scalar and electromagnetic fields.

2 Results

In this section, we explore various avenues to determine whether they have the potential to provide an oscillating scenario (γ).

2.1 The setup

If we have a vacuum region surrounding any spherically symmetric matter distribution, and we describe this vacuum region with a metric, there exist coordinates in which the metric takes the standard Schwarzschild form, with a parameter M_0 equal to the enclosed interior mass. This holds true even when the vacuum region itself is embedded in a spherically symmetric distribution of matter, as verified in [28]. It is important to note that when considering specific scenarios, we must be careful in interpreting Birkhoff's theorem (see Appendix **A** for a discussion). For a metric with the diagonal line element:

$$ds^2 = -A(r)dt^2 + B(r)dr^2 + r^2d\Omega^2 \quad (2.1)$$

with a priori arbitrary functions $A(r)$ and $B(r)$, we can consider a thin spherical shell by first considering a shell with mass density $\rho(r)$ and finite thickness, which supports tangential pressure $p(r)$. However, there is no radial pressure component. If the shell consists of this specific "fluid" with zero radial stress and non-zero compressive stress, it is possible to have a static system. If the radial stress did not vanish, it would be required that at the boundaries with interior and exterior vacua, the stress matches to zero. In this model, the components of the energy-momentum tensor within the shell are $T_{\mu\nu} = \text{diag}(\rho A, 0, pr^2, pr^2 \sin^2 \theta)$. In this scenario, in the interior region, one obtains [28]

$$ds^2 = -\frac{r_S - 2(m_i + m_S)G_N}{r_S - 2m_i G_N} \left(1 - \frac{2m_i G_N}{r}\right) dt^2 + \frac{dr^2}{1 - \frac{2m_i G_N}{r}} + r^2 d\Omega^2. \quad (2.2)$$

The metric in the exterior region is

$$ds^2 = - \left(1 - \frac{2(m_i + m_S)G_N}{r} \right) dt^2 + \frac{dr^2}{1 - \frac{2(m_i + m_S)G_N}{r}} + r^2 d\Omega^2. \quad (2.3)$$

Here, $d\Omega^2 = d\theta^2 + \sin^2\theta d\phi^2$, m_i is the enclosed mass, m_S is the mass of the shell, and r_S is the radial position of the shell. This is the metric we will consider in our calculations, while setting the mass inside the shell m_i to zero ($m_i = 0$). When $m_i = 0$, the spacetime inside the cavity is flat rather than Schwarzschild. When $m_i \neq 0$, one could perform a coordinate rescaling of "t" component (or equivalently set $\frac{r_S - 2(m_i + m_S)G_N}{r_S - 2m_i G_N}$ to 1) to recover the Schwarzschild line element. However, this would be incorrect while leaving the line element outside the shell unchanged, as it would lead to an unphysical discontinuity in the time coordinate and in $A(r)$ across the shell. Now, the line elements read

$$ds^2 = - \frac{r_S - 2m_S G_N}{r_S} dt^2 + dr^2 + r^2 d\Omega^2, \quad \text{in the interior and,} \quad (2.4)$$

$$ds^2 = - \left(1 - \frac{2m_S G_N}{r} \right) dt^2 + \frac{dr^2}{1 - \frac{2m_S G_N}{r}} + r^2 d\Omega^2, \quad \text{in the exterior.} \quad (2.5)$$

Next, we outline the equations of motion (EOM) for the shell presented in [29] with this metric and explore its implications on the existence of a minimal radius within which the shell is not able to collapse further. The metric enters the derivation of the EOM through the Christoffel symbols. The relevant Christoffel symbols are: $\Gamma_{tt}^r = \frac{m_S G_N}{r^2}$, $\Gamma_{rr}^r = 0$. Following the prescription of Israel, we can obtain the normal interior and exterior acceleration. Similarly to the Israel situation, we have the Schwarzschild manifold in the exterior, however in the interior, the time-time component of the metric has the prefactor $h(t) = \frac{r_S - 2m_S G_N}{r_S}$. To consider a variable radius of the shell we denote

$$r_S = R(s). \quad (2.6)$$

Here, s is proper time measured along the streamlines [30]. If we denote the ξ as intrinsic coordinates of the smooth hypersurface Σ in Riemannian manifold V , and ds an infinitesimal displacement in Σ , we can define $u^\alpha = \frac{d\xi^\alpha}{ds}$ as streamlines of the dust particles, following the notation of Israel [30].

We will denote the derivatives with respect to s with a dot. Using the velocities of the shell and normal vectors from the exterior region $u_+^a = \frac{dx_+^a}{ds}$, n_a^+ , and from the interior

$u_-^a = \frac{dx_-^a}{ds}$, n_a^- , we can obtain

$$\text{the exterior:} \quad \mathbf{a}_+ = n_\alpha \frac{\delta u^\alpha}{\delta s} \Big|_+ = n_a \frac{du_+^a}{ds} \mathbf{n}, \quad (2.7)$$

$$\text{and the interior:} \quad \mathbf{a}_- = n_\alpha \frac{\delta u^\alpha}{\delta s} \Big|_- = n_a \frac{du_-^a}{ds} \mathbf{n} \quad (2.8)$$

normal acceleration. This leads to the exterior normal acceleration equivalent to the standard Israel result.

$$a_+ = \frac{\ddot{R} + \frac{m_S G_N}{R^2}}{(1 + \dot{R}^2 - \frac{2m_S G_N}{R})^{1/2}}, \quad (2.9)$$

while for the interior acceleration we obtain

$$a_- = \frac{1}{\sqrt{1 - \frac{2m_S G_N}{R}}} \left(\frac{\ddot{R}}{\sqrt{\dot{R}^2 + 1}} - \frac{m_S G_N \sqrt{1 + \dot{R}^2}}{R(2m_S G_N - R)} \right). \quad (2.10)$$

If we now consider the radial Israel equation [30]

$$n_\alpha \frac{\delta u^\alpha}{\delta s} \Big|_+ + n_\alpha \frac{\delta u^\alpha}{\delta s} \Big|_- = 0 \quad (2.11)$$

we can insert the values for the \mathbf{a}_- and \mathbf{a}_+ to obtain the EOM for the spherical shell of dust which combines exterior and interior, $\mathbf{a}_+ + \mathbf{a}_- = 0$. As we commented above, this configuration can only be stabilized if the stress energy tensor provides some tangential pressure. In our considerations, the role of stabilization will be taken by the Casimir force in the radial direction, i.e. the vacuum fluctuations.

2.2 Massless scalar field

We wish to incorporate the effect of quantum vacuum fluctuations on the motion of the shell. In the low curvature non-relativistic regime this can be achieved by adding the corresponding Casimir force to the Israel's radial equation of motion of a shell. Casimir energy in three dimensions, since it is odd number of dimensions will be finite, [13].

First, let's define the Casimir pressure P as F divided by the surface area $A = 4\pi R^2$

$$P \equiv \frac{F}{A}. \quad (2.12)$$

The Force, in turn, is given from the radial change in the Casimir energy E

$$P = -\frac{1}{4\pi R^2} \frac{\partial E}{\partial R}. \quad (2.13)$$

The Casimir energy E is the sum of Casimir energies E_{in} and E_{out} for the inside and the outside of the shell. We are going to denote the contribution of Casimir pressure with

$$P = \frac{cC\hbar}{8\pi R^4}, \quad (2.14)$$

where C is a numerical constant. From here on, we are going to set $\hbar = 1 = c$. To implement Casimir energy, we assume that:

(i) Backreactions are sub-leading contributions. This means that on the one hand, the space-time curvature is dominated by the mass of the shell, recognizing that Casimir energies typically much smaller than the energy corresponding to the rest mass. Thus, the local Casimir energy does not contribute to the total energy-momentum tensor appearing in Einstein's field equations. On the other hand one also treats the background metric that is used to calculate the Casimir energy as approximately flat. In any realistic scenario, both approximations are perfectly reasonable.

(ii) In the regime of the above assumptions, the Casimir force is introduced as an additional term in the equations of motion, rendering the treatment non-relativistic.

Under these assumptions, the gravitational collapse of a shell in the presence of the Casimir force is described by [31]

$$M \left[\frac{1}{2} (a_+ + a_-) \right] = (4\pi R^2) P, \quad (2.15)$$

where $m_S = M$ is the total proper mass of the shell, the term in square brackets represents the mean acceleration and the right-hand side of the last equation represents the force. Note also that the last equation is reduced to the simplest case by neglecting the Casimir force. This approach, for the scenario when the metric in the interior is $diag(-1, 1, 1, 1)$, can be found in [27]. Now, combining (2.14), (2.15) and M , we can write the EOM as

$$\frac{1}{2} \sigma (a_+ + a_-) = \frac{C}{8\pi R^4}, \quad (2.16)$$

where σ is the mass density per unit area (i.e., $\sigma \equiv M/A$). Multiplying by $2/\sigma$ and

writing the accelerations explicitly one gets

$$\frac{m_S G_N \sqrt{1 - \frac{2m_S G_N}{R}} \sqrt{\dot{R}^2 + 1}}{(R - 2m_S G_N)^2} + \frac{\ddot{R}}{\sqrt{1 - \frac{2m_S G_N}{R}} \sqrt{\dot{R}^2 + 1}} + \frac{\frac{m_S G_N}{R^2} + \ddot{R}}{\sqrt{-\frac{2m_S G_N}{R} + \dot{R}^2 + 1}} = \frac{C}{m_S R^2}. \quad (2.17)$$

The Casimir force ordinarily includes its two-loop radiative corrections. However, these corrections do not account for significant differences in the dynamics of the system and will thus be neglected in further analysis.

We wish to investigate the existence of a minimal radius resulting from the interplay between the inward-pointing gravitational force and the outward-pointing Casimir force. To do so, we make the simplifying assumption that the initial velocity of the shell is $\dot{R} = 0$, an

$$\left[\frac{m_S G_N}{R^2} \left(1 + \frac{1}{\left(1 - \frac{2m_S G_N}{R} \right)} \right) + 2\ddot{R} \right] \frac{1}{\sqrt{1 - \frac{2m_S G_N}{R}}} = \frac{C}{m_S R^2}. \quad (2.18)$$

Further, we are only interested in dynamics well outside the Schwarzschild radius $R > 2m_S G_N$, where both the Newtonian and non-relativistic approximations can be trusted, and neglecting backreactions is well justified. In this limit, we can expand the left-hand side of (2.18) in inverse powers of R . This yields the equation for slow motions in the far region:

$$\ddot{R} = \frac{3G_N m_S (C + 2G_N m_S^2) - 2(C - 2G_N m_S^2)R}{2m_S R^4}. \quad (2.19)$$

The “far region” is defined by

$$R \ll 2m_S G_N. \quad (2.20)$$

Now, we seek for a stability condition. One necessary condition for a stable configuration γ) is the existence of a “rest” radius R_r which has vanishing acceleration

$$\ddot{R}|_{R=R_r} = 0. \quad (2.21)$$

For the case of (2.19), this condition is solved by

$$R_r = \frac{G_N m_S (C + 2G_N m_S^2)}{C - 2G_N m_S^2}. \quad (2.22)$$

The second condition for stability, is that the dynamics is attractive towards the rest radius, in some finite vicinity of R_r . This condition implies

$$\left. \frac{d(\ddot{R})}{dR} \right|_{R_r} < 0. \quad (2.23)$$

Using (2.22) to evaluate the left hand side of (2.23) we find

$$\left. \frac{d(\ddot{R})}{dR} \right|_{R_r} = \frac{(C - 2G_N m_S^2)^4}{2G_N^3 m_S^4 (C + 2G_N m_S^2)^3} > 0. \quad (2.24)$$

We remember that $C > 0$. Thus, (2.24) is in contradiction with (2.23), which means that a stable balance between the Casimir force and the gravitational dynamics is not possible in the Newtonian regime of a massless scalar particle (2.17). A numerical analysis shows that the same is true if one explores slow motion for all radii $R > 2m_S G_N$. This can nicely be exemplified with figure 1. Since in the true Casimir effect $C < 0.1$, all scenarios where the shell is heavier than the Planck mass are represented by the green curve. Light shells instead $m_S^2 < C/(2G_N)$, would be represented by the blue or orange curve in figure 1. In any case, the stability condition (2.23) is never fulfilled in the massless case. This means that in this case it is not possible to realize scenario γ (only α or β)).

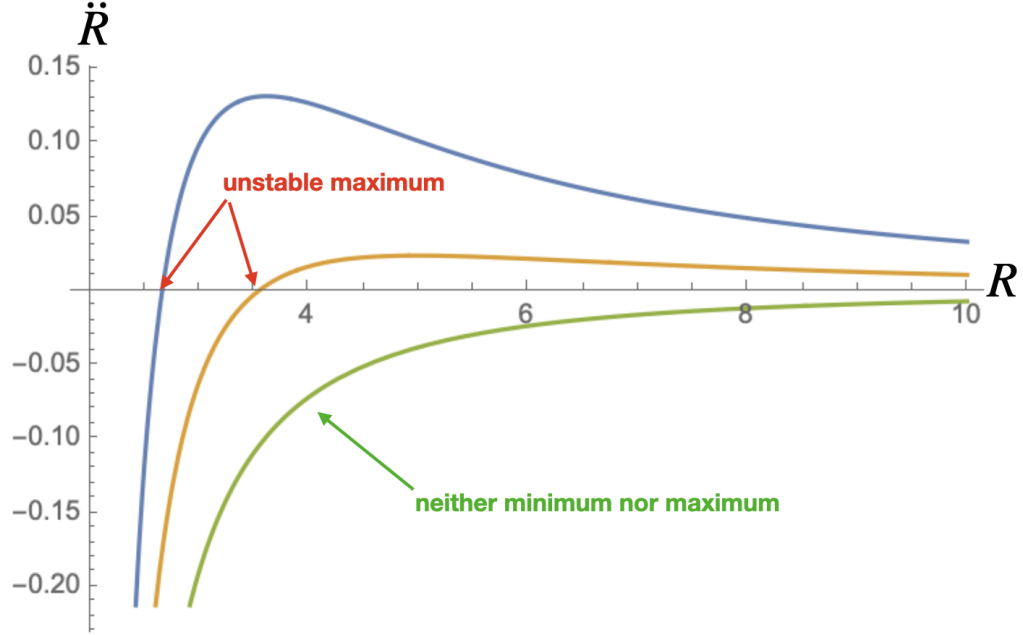


Figure 1: \ddot{R} as a function of R for (2.17). The parameters are chosen to be $G_N = m_S = 1$. The blue, orange, green curves are for values of $C = 10, 5, 1$.

2.3 Massive scalar field

In the previous section, we explored the influence of the Casimir force of a massless scalar field on the dynamics of the gravitational collapse of a shell. The analysis shows that there exists no stable minimal radius. We now expand the EOM to include the Casimir force for a massive scalar field. The force is pointed outward and has magnitude [23, 32]

$$F_{\text{massive}} = \sum_{j=1}^{\infty} \frac{(-1)^{j+1} \left(\mathbf{H}_2(2\pi j m_\phi R) + \frac{4j m_\phi R}{3} - I_2(2\pi j m_\phi R) \right)}{j} \quad (2.25)$$

where m_ϕ is the mass of the scalar field. The outcome of the regularization of the sum (2.25) can be evaluated numerically. This result is well fitted by the phenomenological function of the dimensionless product of radius R and energy as a function of the dimensionless product of mass m_ϕ times radius R

$$RE_m = \frac{a + b(Rm_\phi)}{1 + c(Rm_\phi) + d(Rm_\phi)^3}. \quad (2.26)$$

Where the resulting dimensionless fitting parameters are $a = 0.0029$, $b = 0.0674$, $c = 16.28$, $d = 57.55$. This fit is shown in figure 2. Equipped with this relation, we can

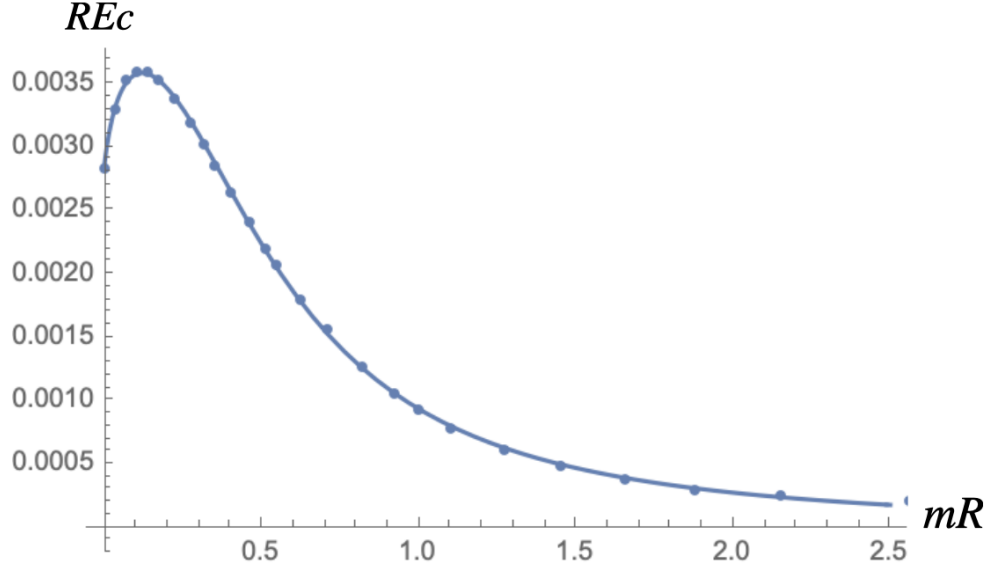


Figure 2: Casimir force in a spherical shell produced by a massive scalar field. The points are the numerical results given in [12]. The continuous curve is the fit given in equation (2.26).

proceed to calculate the Casimir force via

$$F_{m_\phi} = -\frac{dE_m}{dR}. \quad (2.27)$$

This force is then divided by the mass of the shell m_S and inserted on the RHS of the relations (2.17 and 2.18). This gives the equation of motion for the shell with non-relativistic velocities

$$\ddot{R} = \frac{a + m_\phi R(2ac + m_\phi R(bc + dm_\phi R(4a + 3bm_\phi R)))}{2m_S R^2(1 + cm_\phi R + dm_\phi^3 R^3)^{3/2}} \sqrt{1 - \frac{2m_S G_N}{R}} - \frac{G_N m_S}{2R^2} - \frac{G_N m_S}{2R^2(1 - \frac{2G_N m_S}{R})}. \quad (2.28)$$

The radii with vanishing acceleration are found by imposing (2.21). This can be solved analytically in the far region, yielding

$$r_S = \frac{\sqrt{6bdG_N m_S^2 m_\phi^2 - 7d^2 G_N^4 m_S^6 m_\phi^4 - dG_N^2 m_S^3 m_\phi^3}}{2dG_N m_S^2 m_\phi^2}. \quad (2.29)$$

For consistency, we have to demand that this radius is both real and much larger than the Schwarzschild radius of the mass m_S . Interestingly, this implies an upper limit for the mass of the shell as a function of m_ϕ

$$m_S^4 < \frac{3b}{16dG_N^3 m_\phi^2}. \quad (2.30)$$

Next we have to check whether the point of vanishing acceleration is actually stable. This condition can be implemented in terms of the relation (2.23). In this region we find

$$\left. \frac{d\ddot{R}}{dR} \right|_{r_S} = 16d^4 G_N^5 m_S^9 m_\phi^8 \frac{G_N m_S \sqrt{dG_N m_S^2 m_\phi^2 (6b - 7dG_N^3 m_S^4 m_\phi^2) + 7dG_N^3 m_S^4 m_\phi^2 - 6b}}{(\sqrt{dG_N m_S^2 m_\phi^2 (6b - 7dG_N^3 m_S^4 m_\phi^2)} - dG_N^2 m_S^3 m_\phi^2)^5}. \quad (2.31)$$

The right hand side of this relation is negative if

$$m_S^4 < \frac{6b}{7dG_N^3 m_\phi^2}, \quad (2.32)$$

which is already assured by imposing (2.30). Thus, from the analytic approximations (2.29-2.31) we conclude that the Casimir force for massive fields could produce a meta-stable configuration (in the sense of dependence on the initial conditions) in the interplay with the gravitational attraction, if the condition (2.30) is satisfied.

Next, we proceed to check this analytical intuition numerically by plotting (2.28) as a function of R . The result is shown in Figure 3.

To get an idea of which type of shells could be stabilized, let's assume that the stabilizing scalar field is the Higgs field with $m_\phi = 125$ GeV. The Casimir force for this field could stabilize, under the right initial conditions, a spherical shell with a mass smaller than $m_S < 10^{25}$ GeV ≈ 0.2 kg. However, the stable radius for this configuration would be eight orders of magnitude smaller than the proton radius. This is extremely small, even though it is still three orders of magnitude larger than the Schwarzschild radius of this

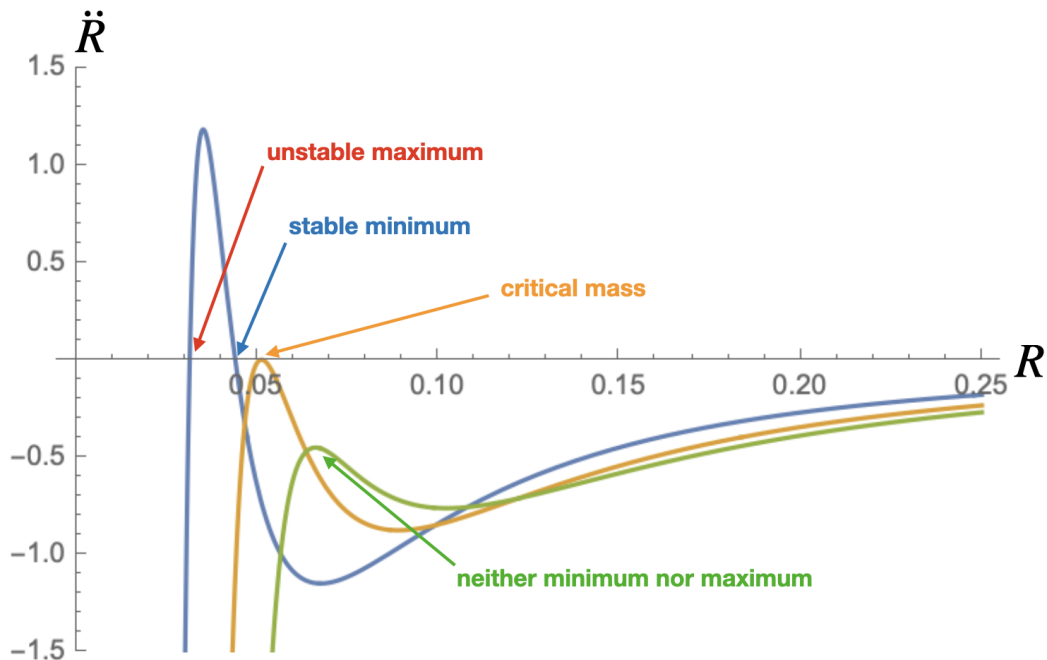


Figure 3: Acceleration (2.28) as a function of R in Planck units $G_N = 1$ and fixing $m_S^2 m_\phi = 0.007$. The blue curve is for $m_S = 0.01$. The orange curve is for $m_S = 0.015$. The green curve is for $m_S = 0.25$. The zeros of these curves are the solutions of $\ddot{R} = 0$. Only the blue curve has a meta-stable configuration.

configuration.

This result can be seen from two perspectives. On the one hand, it is encouraging because it could be interpreted as a hint of a mechanism stabilizing the gravity-matter interplay at very high densities. On the other hand, it applies classical mechanics at distance scales that are deeply quantum. Thus, even though we found a scenario that realizes the stable scenario γ), it has to be taken with a big grain of salt.

Note that another candidate for scalar fields could be cosmological fields such as the inflaton. These could provide very different masses and radii. However, since we do not know how to implement boundary conditions for this field, we do not explore this possibility further at this point.

2.4 Temperature dependence

In this section, we consider if there is a balance of the thin spherical shell and the repulsive Casimir force due to the fluctuation of massless scalar fields in the sphere at non-vanishing

temperature. To model this behavior, we are going to use the acceleration from the interior and the exterior of the shell as above, while on the right-hand side, we implement the contribution from the Casimir force at finite temperature. The Casimir energy of the thin spherical shell in the limit of low and high temperature has been studied, and a review can be found in [13].

2.4.1 High temperature for scalar field

In the high temperature limit, the EOM for the shell is given by

$$\frac{\ddot{R} + \frac{m_S G_N}{R^2}}{(1 + \dot{R}^2 - \frac{2m_S G_N}{R})^{1/2}} + \frac{1}{\sqrt{1 - \frac{2m_S G_N}{R}}} \left(\frac{\ddot{R}}{\sqrt{\dot{R}^2 + 1}} - \frac{m_S G_N \sqrt{1 + \dot{R}^2}}{R(2m_S G_N - R)} \right) = -\frac{1}{m_S} \frac{T}{24R} \quad (2.33)$$

Like before, we are interested in the slow motion regime, for which we impose $\dot{R} = 0$. Furthermore, we remember that the entire classical approach without backreaction is only reliable in the Newtonian regime $R \gg m_S G_N$. In this expansion, we get from (2.33)

$$\ddot{R} = -\frac{1}{m_S} \frac{T}{24R} - G_N \frac{m_S}{R^2}. \quad (2.34)$$

From this expansion, it becomes clear that in the high-temperature limit, both the gravitational and the Casimir interactions contribute to an inwards-directed pull. Thus, in this regime, no stable configuration is possible; instead, only scenario α) is realized.

2.4.2 Low temperature for scalar field

The Casimir energy for a scalar field in the low temperature is [13],

$$\Delta_T \mathcal{F}^D = \frac{\pi^3 R}{6} (k_B T)^2 - \zeta_R(3) R^2 (k_B T)^3.$$

Here, the index D denotes Dirichlet boundary conditions imposed on the sphere. The Boltzman constant is denoted with k_B and $\zeta_R(3)$ is the Riemman zeta function. Combining the energy at zero temperature and the thermal correction, we obtain the total contribution from Casimir energy at low temperature. That gives the corresponding radial force acting on the spherical shell, which we insert on the right-hand side of the equation.

This leads to

$$\begin{aligned} \frac{\ddot{R} + \frac{m_S G_N}{R^2}}{(1 + \dot{R}^2 - \frac{2m_S G_N}{R})^{1/2}} + \frac{1}{\sqrt{1 - \frac{2m_S G_N}{R}}} \left(\frac{\ddot{R}}{\sqrt{\dot{R}^2 + 1}} - \frac{m_S G_N \sqrt{1 + \dot{R}^2}}{R(2m_S G_N - R)} \right) = \\ = \frac{C}{m_S R^2} - \frac{\frac{1}{6}\pi^3 T^2 - 2RT^3 \zeta(3)}{m_S} \end{aligned} \quad (2.35)$$

In the limit $T \rightarrow 0$, the EOM reduces to the case of a temperature independent massless scalar field.

As in the previous cases we investigate the conditions for which $\ddot{R} = \dot{R} = 0$. The stable $R > 0$ solutions for which this conditions are satisfied would be the sought after minimal radii R_{\min} . Again, we first impose $\dot{R} = 0$ and solve for \ddot{R}

$$\begin{aligned} \ddot{R} = \frac{1}{2} \sqrt{1 - \frac{2m_S G_N}{R}} \left[\frac{\frac{C}{R^2} - (\frac{1}{6}\pi^3 T^2 - 2RT^3 \zeta(3))}{m_S} - \frac{m_S G_N}{R \sqrt{1 - \frac{2m_S G_N}{R}}} \left(\frac{1}{R} - \frac{1}{2m_S G_N - R} \right) \right] \\ \approx \frac{T^2}{m_S G_N R^2} \left[\frac{C - G_N m_S^2}{T^2} - \frac{\pi^3 R^2}{12} + \frac{R^3 T \zeta(3)}{1} \right]. \end{aligned} \quad (2.36)$$

Before solving the right hand side for $\ddot{R} = 0$, let's discuss the apparent properties of these three roots. Since the leading term in the bracket $\sim R^3$ is positive, the largest positive root will always be unstable. If the $\sim cte.$ term is also positive, there can be two positive roots, from which the smaller one would be stable. If the $\sim cte.$ term is negative, there could be one or three real roots. In the former case, the root is unstable. The latter case does not happen because if at some radius the $\sim R^2$ term dominates, it does so for positive and negative R , in particular since there is no $\sim R$ term. The analytic expressions for the roots of the above equation (2.36) we present in (4.1), in the Appendix. The number of real roots can be shown to only depend on the parameter m_S . In Figure 4 we plot $(T \cdot (4.1))$ as a function of the dimensionless ratio $m_z / \sqrt{G_N}$. Figure 4 shows nicely that a stable solution is only possible for light shells, as long as $C > G_N m_S^2$. To illustrate this effect, we plot \ddot{R} as a function of R , for different temperatures. In the right panel, we plotted the case where condition $C > G_N m_S^2$ does hold, whereas in the left panel we plot the case where this condition does not hold.

Looking at the first panel of Fig.(5), we see the effect of including temperature corrections on the evolution of the acceleration. For the large m_S , the behavior is similar to the zero temperature case, and the main difference appears for a small shift on the peak of the

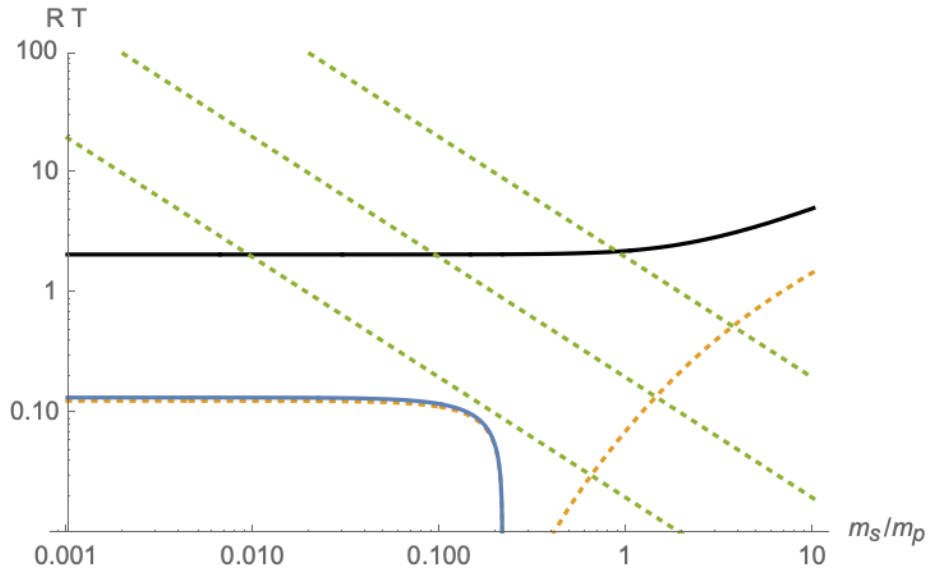


Figure 4: Value of the roots TR_i as a function of m_S/m_p , where $m_p = 1/\sqrt{G_N}$. The black line is the solution R_1 , the blue line is the stable solution R_3 . The solution R_2 is only plotted as dotted line, because for $m_S^2 < G_N$ it is negative and for $m_S^2 > G_N$ it is imaginary. The green lines are $1/(m_S 200)$, $1/(m_S 20)$, $1/(m_S 2)$. They represent the underlying criterium of large radius expansion, namely that we only should trust scenarios below the green line which means temperatures below the Planck energy.

acceleration. From the second panel of Fig.(5) we confirm that a stable configuration can be found for small m_S , even when no large radius expansion is imposed. The stability can be seen from the fact that the radial acceleration is negative for $R > R_{\min}$ and positive for $R < R_{\min}$. Therefore, the interplay between the temperature dependent Casimir force of a massless scalar field with the gravitational attraction caused by the massive shell, can stabilize the system, which corresponds to scenario γ).

2.4.3 Electromagnetic Casimir at low temperature and large $R \gg r_S$

Since the scalar Casimir effect at low temperatures yielded the desirable scenario γ), it is reasonable to hope for a similar result when electromagnetic interactions are considered. The low-temperature corrections to the electromagnetic Casimir effect are, however, simply $\sim T^4$ [13]. Thus, the motion of the shell is described by

$$\ddot{R} = \frac{C}{m_S R^2} - G_N \frac{m_S}{R^2} + \frac{1}{5} \pi^3 R^2 (k_B T)^4. \quad (2.37)$$

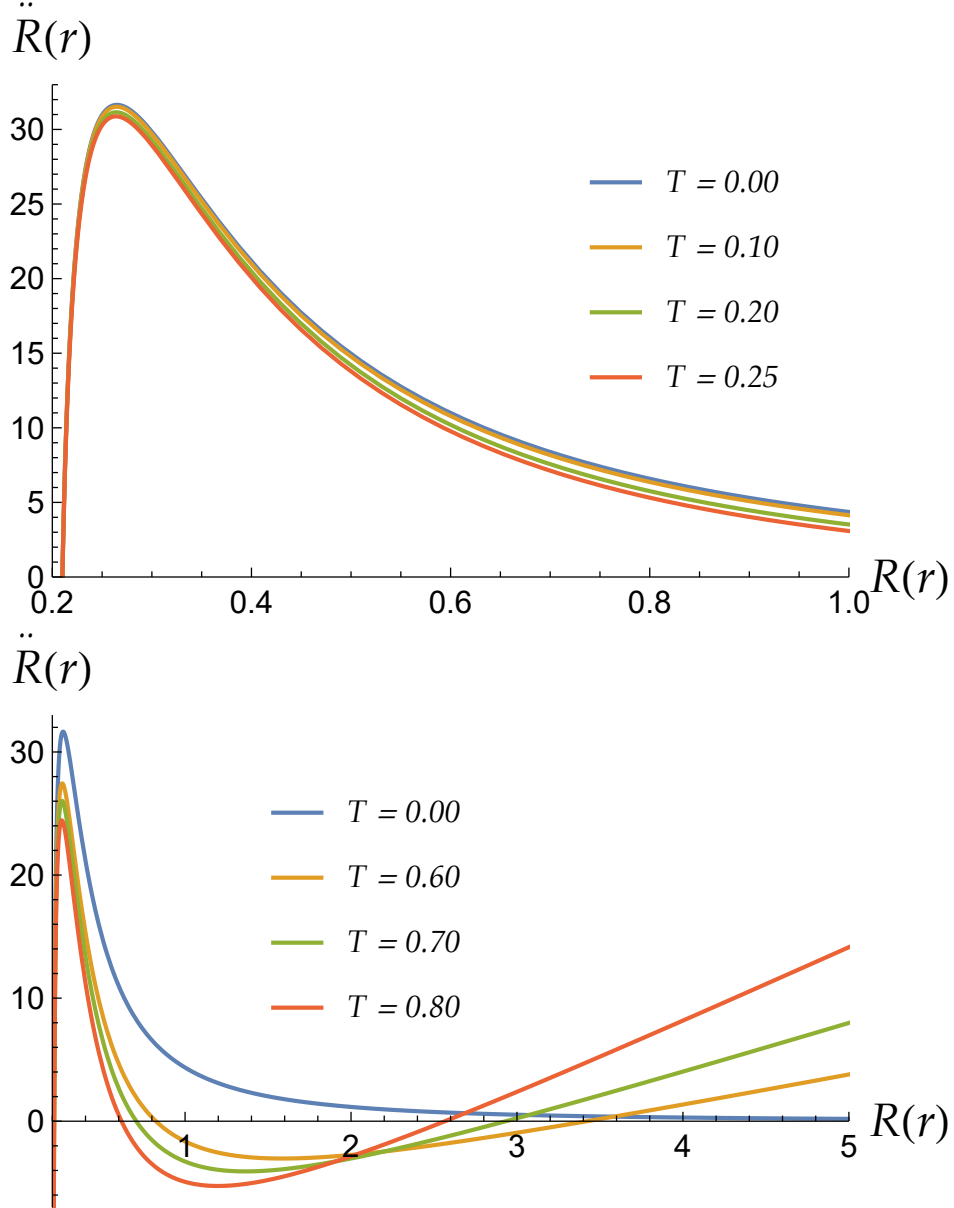


Figure 5: **First panel:** Radial acceleration \ddot{R} versus R , assuming four (small) different temperature values. **Second panel:** Radial acceleration \ddot{R} versus R at four different (moderate) temperature values. We also plotted the zero-temperature case for comparison. For illustrative purposes, we have used the mass $m_S = 0.1$, $G_N = 1$, and $C = 1$ and further $k_B = \hbar = 1$.

The radius with zero acceleration is

$$R_0^2 = \frac{\sqrt{5}\sqrt{G_N m_S^2 - C}}{k_B^2 \sqrt{m_S} \pi^{3/2} T^2}. \quad (2.38)$$

The stability criterium at this radius is

$$\left. \frac{d\ddot{R}}{dR} \right|_{R_0} = 4k_B^3 \frac{(G_N m_S - C/m_S)^{1/4} \pi^{9/4} T^3}{5^{3/4}} > 0. \quad (2.39)$$

Thus, if $m_S^2 < C/G_N$, the configuration always explodes, which corresponds to scenario β). Instead, if $m_S^2 > C/G_N$, the configuration is unstable in the sense that it depends on the initial condition, whether the outcome is the scenario α) or β). A stable scenario γ) is not possible here.

3 Conclusion

In the present work, we have investigated the dynamics of the gravitational collapse of a shell in the presence of the Casimir force in four dimensions considering different types of vacuum fluctuations:

- i) massless scalar fields,
- ii) massive scalar fields,
- iii) massless scalar fields at high temperature limit,
- iv) massless scalar fields at low temperature limit,
- v) electromagnetic fields at low temperature limit.

Specifically, we have investigated, among other things, the existence of a minimal radius as a result of the interplay between the inward-pointing gravitational force and the outward-pointing Casimir force. We defined the minimal radius as the point at which the acceleration and velocity of the collapsing shell can reach $\dot{R} = 0 = \ddot{R}$. To evaluate the stability of the minimal radius R_{\min} , we explored the derivatives of the acceleration \ddot{R} with respect to the radius R at this point of interest. Finally, we have illustrated our results with some figures.

In two out of the five scenarios that we analyzed we obtain the stable region, while in the other three scenarios no stability region is found: (i) when the Casimir force is produced by the massless scalar particles at the zero temperature, there is no radius at which the thin spherical shell would oscillate around a minimum. (ii) When the Casimir force is caused by massive scalar particles, the stable region is obtained when the mass shell is lighter than the fluctuating massive particle. (iii) For the thin spherical shell of the mass m_S with the massless scalars at the low non-zero temperature, we obtain a stable region. The region satisfies the conditions that the radius of the shell is bigger than the two masses of the shell, $R > 2m_S$, and that low-temperature behavior for the thermal corrections can be used $k_B T R \ll 1$ [13]. (iv) In the limit when the Casimir energy is expanded around a high-temperature limit, we do not obtain a stable region. The same negative result is true for the electromagnetic Casimir effect in the low temperature limit (v).

Note that due to the large theoretical uncertainties on the interplay between quantum effects and general relativity we chose to study this simple model in the regime where we can expect that all assumptions still hold, namely in the regime of weak gravity and non-relativistic motion. In this regime, we do not find realistic scenarios on our model, where the Casimir force could stabilize a shell against the gravitational pull.

4 Acknowledgements

The work of IL was supported by the Hertha Firnberg grant T1269-N and Elise Richter grant V 1052-N by the Austrian Science Fund, FWF. A. R. acknowledges financial support from the Generalitat Valenciana through PROMETEO PROJECT CIPROM/2022/13. A. R. is funded by the María Zambrano contract ZAMBRANO 21-25 (Spain) (with funding from NextGenerationEU).

Appendix

A Remark on Birkhoff's theorem

According to Birkhoff's theorem [33], in Einstein's theory of relativity, when we have a symmetric mass distribution that is not rotating in empty space we can describe the

gravitational field outside this distribution using the Schwarzschild metric. In essence, this metric enables us to simplify the understanding and calculation of effects in several situations and has important implications. Birkhoff's theorem can be seen as a characterization of the structure of vacuum spacetimes that exhibit local spherical symmetry. Its significance lies in the fact that it serves not only as a classical cornerstone of general relativity but also as a vital tool in the fields of gravitational physics and cosmology. In particular, Birkhoff's theorem is conventionally employed for the following purposes: i) to establish that the empty spacetime within a spherically symmetric mass shell corresponds to Minkowski spacetime, ii) to demonstrate that spherical gravitational collapse does not emit gravitational waves, iii) to finalize the proof of the classical uniqueness theorem for static black holes [34]. Given its significance, it becomes evident that Birkhoff's theorem plays a crucial role in the context of spherically symmetric spacetimes within the framework of general relativity.

There is some discussion in the literature concerning the applicability and validity of Birkhoff's theorem. In particular, Israel [29] and Brevik [27] used the Birkhoff theorem to derive the corresponding equations of motion (EOMs) describing the gravitational collapse of a thin shell. However, Zhang and Yi [35] pointed out that there is a misunderstanding in the interpretation of the Birkhoff theorem and that the original result of [29] is questionable. They argue that the correct metric, which is continuous with the location of an external observer, is determined by both the enclosed mass and the mass distribution outside. The statements in the work by Zhang and Yi were elaborated in [28] where it was demonstrated that the Birkhoff's theorem holds using a traditional metric-based approach. They also show that it holds at the level of tetrad components. What they consider does not depend on the distribution of matter in the interior or exterior regions, or state of motion of the system, under the assumption that spherical symmetry holds. It would be unphysical though to rescale the interior vacuum region and keep the line-element outside of the spherical shell unchanged because it would lead to discontinuity in the time coordinate and corresponding term in the metric element. An additional example of the gravitational field at a certain radius in a spherically-symmetric matter distribution which is outside of the radius has also been analyzed in [36].

Even though, this discussion on the different versions of Birkhoff's theorem is interesting from a theoretical perspective, it is irrelevant for our purposes. The reason for this irrelevance is that in the non-relativistic low curvature limit both versions of the metrics give same result for the stability of the shell in our construction. We decided to follow the

formulation used by ([27, 29]), but in our case, ([28]) would have given the same results.

B Analytic expressions for temperature dependence

The analytic expressions for the roots of the EOM (2.36) are

$$\begin{aligned}
 R_1 &= \frac{1}{36T\zeta(3)} \left(\pi^3 + \frac{\pi^6}{(\pi^9 + 216\zeta(3)(108(G_N - m_S^2)\zeta(3) + \sqrt{(C - G_N m_S^2)(11664(C - G_N m_S^2)\zeta(3) - \pi^9)}))^{1/3}} + \right. \\
 &\quad \left. (\pi^9 + 216\zeta(3)(108(G_N - m_S^2)\zeta(3) + \sqrt{(C - G_N m_S^2)(11664(C - G_N m_S^2)\zeta(3) - \pi^9)}))^{1/3} \right), \\
 R_{2,3} &= \frac{1}{72T\zeta(3)} \left(2\pi^3 + \frac{\mp\pi^6(1 + i\sqrt{3})}{(\pi^9 + 216\zeta(3)(108(G_N - m_S^2)\zeta(3) + \sqrt{(C - G_N m_S^2)(11664(C - G_N m_S^2)\zeta(3) - \pi^9)}))^{1/3}} + \right. \\
 &\quad \left. \pm(1 + i\sqrt{3})(\pi^9 + 216\zeta(3)(108(G_N - m_S^2)\zeta(3) + \sqrt{(C - G_N m_S^2)(11664(C - G_N m_S^2)\zeta(3) - \pi^9)}))^{1/3} \right).
 \end{aligned} \tag{4.1}$$

Interestingly, the temperature factors out of the solutions (4.1), thus the number of real roots only depends on the values of $(C, G_N,$ and $m_S)$. Further, C has a definite value $C = 0.0461766$ [13]. Thus, we can multiply both sides of (4.1) with T to make it a dimensionless identity. Now we can express all dimensionful quantities in Planck units, which leaves m_S as the only parameter which determines the number of real roots.

Bibliography

- [1] Richard Tolman and Paul Ehrenfest. Temperature Equilibrium in a Static Gravitational Field. *Phys. Rev.*, 36(12):1791–1798, 1930.
- [2] Jacob D. Bekenstein. Hydrostatic Equilibrium and Gravitational Collapse of Relativistic Charged Fluid Balls. *Phys. Rev. D*, 4:2185–2190, 1971.
- [3] Marek Nowakowski, Juan-Carlos Sanabria, and Alejandro Garcia. Gravitational equilibrium in the presence of a positive cosmological constant. *Phys. Rev. D*, 66:023003, 2002.
- [4] Pankaj S. Joshi, Daniele Malafarina, and Ramesh Narayan. Equilibrium configurations from gravitational collapse. *Class. Quant. Grav.*, 28:235018, 2011.
- [5] Riccardo Belvedere, Daniela Pugliese, Jorge A. Rueda, Remo Ruffini, and She-Sheng Xue. Neutron star equilibrium configurations within a fully relativistic theory with strong, weak, electromagnetic, and gravitational interactions. *Nucl. Phys. A*, 883:1–24, 2012.
- [6] Juan M. Z. Pretel. Equilibrium, radial stability and non-adiabatic gravitational collapse of anisotropic neutron stars. *Eur. Phys. J. C*, 80(8):726, 2020.
- [7] Charles W. Misner, K. S. Thorne, and J. A. Wheeler. *Gravitation*. W. H. Freeman, San Francisco, 1973.
- [8] S. K. Lamoreaux. The Casimir force: Background, experiments, and applications. *Rept. Prog. Phys.*, 68:201–236, 2005.
- [9] Steven Weinberg. The Cosmological Constant Problem. *Rev. Mod. Phys.*, 61:1–23, 1989.
- [10] Ignacio A. Reyes and Giovanni Maria Tomaselli. Quantum field theory on compact stars near the Buchdahl limit. *Phys. Rev. D*, 108(6):065006, 2023.
- [11] Ignacio A. Reyes. Trace anomaly and compact stars. 8 2023.
- [12] Michael Bordag, U. Mohideen, and V. M. Mostepanenko. New developments in the Casimir effect. *Phys. Rept.*, 353:1–205, 2001.
- [13] M. Bordag, G. L. Klimchitskaya, U. Mohideen, and V. M. Mostepanenko. *Advances in the Casimir effect*, volume 145. Oxford University Press, 2009.
- [14] A. Chodos, R. L. Jaffe, K. Johnson, Charles B. Thorn, and V. F. Weisskopf. A New Extended Model of Hadrons. *Phys. Rev. D*, 9:3471–3495, 1974.

- [15] A. Chodos, R. L. Jaffe, K. Johnson, and Charles B. Thorn. Baryon Structure in the Bag Theory. *Phys. Rev. D*, 10:2599, 1974.
- [16] Ted Barnes, F. E. Close, and F. de Viron. Q anti-Q G Hermaphrodite Mesons in the MIT Bag Model. *Nucl. Phys. B*, 224:241, 1983.
- [17] Eduardo S. Fraga and Leticia F. Palhares. Deconfinement in the presence of a strong magnetic background: an exercise within the MIT bag model. *Phys. Rev. D*, 86:016008, 2012.
- [18] Timothy H. Boyer. Quantum electromagnetic zero point energy of a conducting spherical shell and the Casimir model for a charged particle. *Phys. Rev.*, 174:1764–1774, 1968.
- [19] Roger Balian and Bertrand Duplantier. Electromagnetic Waves Near Perfect Conductors. 2. Casimir Effect. *Annals Phys.*, 112:165, 1978.
- [20] Kimball A. Milton, Lester L. DeRaad, Jr., and Julian S. Schwinger. Casimir Selfstress on a Perfectly Conducting Spherical Shell. *Annals Phys.*, 115:388, 1978.
- [21] Kimball A. Milton. Zero Point Energy in Bag Models. *Phys. Rev. D*, 22:1441, 1980.
- [22] Kimball A. Milton. FERMIONIC CASIMIR STRESS ON A SPHERICAL BAG. *Annals Phys.*, 150:432, 1983.
- [23] Michael Bordag, E. Elizalde, K. Kirsten, and S. Leseduarte. Casimir energies for massive fields in the bag. *Phys. Rev. D*, 56:4896–4904, 1997.
- [24] E. Elizalde, Michael Bordag, and K. Kirsten. Casimir energy for a massive fermionic quantum field with a spherical boundary. *J. Phys. A*, 31:1743–1759, 1998.
- [25] Hamid Haghmoradi, Hauke Fischer, Alessandro Bertolini, Ivica Galić, Francesco Intravaia, Mario Pitschmann, Raphael Schimpl, and René I. P. Sedmik. Force metrology with plane parallel plates: Final design review and outlook. *MDPI Physics*, 6(2), 2024.
- [26] Francesco Alessio, Glenn Barnich, and Martin Bonte. Gravitons in a Casimir box. *JHEP*, 02:216, 2021. [Erratum: *JHEP* 03, 228 (2021)].
- [27] Iver Brevik and Kolbenstvedt Høyve. Casimir effect and gravitational collapse. *Il Nuovo Cimento B (1971-1996)*, 82:71784, 1984.
- [28] Do Young Kim, Anthony N. Lasenby, and Michael P. Hobson. Spherically-symmetric solutions in general relativity using a tetrad-based approach. *Gen. Rel. Grav.*, 50(3):29, 2018.
- [29] W. Israel. Gravitational collapse and causality. *Phys. Rev.*, 153:1388–1393, Jan 1967.

- [30] W. Israel. Singular hypersurfaces and thin shells in general relativity. *Nuovo Cim. B*, 44S10:1, 1966. [Erratum: *Nuovo Cim. B* 48, 463 (1967)].
- [31] D. Vick. Gravitational collapse of a shell subject to the Casimir force. *Nuovo Cimento B Serie*, 94B(1):54–62, January 1986.
- [32] M.A. Valuyan. Casimir energy calculation for massive scalar field on spherical surfaces: an alternative approach. *Canadian Journal of Physics*, 96(9):1004–1009, 2018.
- [33] George David Birkhoff and Rudolph Ernest Langer. *Relativity and modern physics*. 1923.
- [34] Werner Israel. Event horizons in static vacuum space-times. *Phys. Rev.*, 164:1776–1779, 1967.
- [35] SHUANG-NAN ZHANG and SHUXU YI. On a common misunderstanding of the birkhoff theorem and light deflection calculation: Generalized shapiro delay and its possible laboratory test. *International Journal of Modern Physics: Conference Series*, 12:419–430, 2012.
- [36] Roshina Nandra, Anthony Lasenby, and Michael Hobson. Dynamics of a spherical object of uniform density in an expanding universe. *Phys. Rev. D*, 88(4):044041, 2013.